Chinese Journal of Catalysis 41 (2020) 350–356

available at www.sciencedirect.com

ScienceDirect

journal homepage: www.elsevier.com/locate/chnjc

Article

Promotion effects of nickel-doped Al_2O_3-nanosheet-supported Au catalysts for CO oxidation

Rao Lu, Lei He, Yang Wang, Xin-Qian Gao, Wen-Cui Li *

State Key Laboratory of Fine Chemicals, School of Chemical Engineering, Dalian University of Technology, Dalian 116024, Liaoning, China

ARTICLE INFO

Article history:
Received 10 May 2019
Accepted 23 June 2019
Published 5 February 2020

Keywords:
Alumina
Gold catalyst
Nickel doping
CO oxidation
Oxygen activation

ABSTRACT

Supported gold catalysts show high activity toward CO oxidation, and the nature of the support significantly affects the catalytic activity. Herein, serial Ni doping of thin porous Al_2O_3 nanosheets was performed via a precipitation-hydrothermal method by varying the amount of Ni during the precipitation step. The prepared nanosheets were subsequently used as supports for the deposition of Au nanoparticles (NPs). The obtained Au/Ni_xAl catalysts were studied in the context of CO oxidation to determine the effect of Ni doping on the supports. Enhanced catalytic performances were obtained for the Au/Ni_xAl catalysts compared with those of the Au supported on bare Al_2O_3. The Ni content and pretreatment atmosphere were both shown to influence the catalytic activity. Pretreatment under a reducing atmosphere was beneficial for improving catalytic activity. The highest activity was observed for the catalysts with a Ni/Al molar ratio of 0.05, achieving complete CO conversion at 20 °C with a gold loading of 1 wt%. The in-situ FTIR results showed that the introduction of Ni strengthened CO adsorption on the Au NPs. The H_2-TPR and O_2-TPD results indicated that the introduction of Ni produced new oxygen vacancies and allowed the oxygen molecules to be adsorbed and activated more easily. The improved catalytic performance after doping Ni was attributed to the smaller size of the Au NPs and more active oxygen species.

1. Introduction

Supported gold catalysts have attracted significant attention due to their potential applications in many low-temperature reactions of industrial and environmental importance [1], such as CO oxidation [2], the water gas shift (WGS) reaction [3], selective oxidation of organic compounds [4], and VOC removal [5]. In particular, CO oxidation is the most extensively studied owing to its practical applications and its status as a model reaction for probing the oxidation activity and determining reaction mechanisms [6]. It is well known that the catalytic activity of Au catalysts is strongly dependent on the nature of its support [7–9]. Generally, Au nanoparticles (NPs) supported on reducible oxides (including TiO_2 [10] and CeO_2 [11]) exhibit excellent activity for CO oxidation. Strong metal-support interaction between the Au NPs and supports stabilizes the small Au NPs and creates active sites at the interfaces [12]. Moreover, the supports act as electron modifiers providing new active sites or function as active species during the catalytic reaction. These catalysts have been widely studied, but most are not suitable for large-scale applications for various reasons [13].

Although Al_2O_3 is considered to be an inert support for CO oxidation due to its non-reducibility and relatively weak interactions with gold, it is a preferable support from a practical point of view due to its high specific surface area, excellent thermal and mechanical stability, and relative inertness toward steam. By improving the synthesis method, morphology, and surface defects, more "active" Al_2O_3 supports can be produced

* Corresponding author. Tel: +86-0411-84986355; E-mail: wencuili@dlut.edu.cn
DOI: S1872-2067(19)63439-X | http://www.sciencedirect.com/science/journal/18722067 | Chin. J. Catal., Vol. 41, No. 2, February 2020

for Au catalysts [14]. Previously, Al_2O_3 rods with abundant external mesopores were successfully synthesized and the corresponding 3 wt% Au/Al_2O_3 catalyst exhibited excellent catalytic activity for CO oxidation, achieving complete CO conversion at 18 °C [15]. Alternatively, adding transition metals or metal oxides can enhance the activity of Au catalysts by adjusting the electronic properties of Au and promoting oxygen activation during the reaction [16–18]. Nickel-based oxides have been developed as active materials for CO oxidation. For example, nanosized nickel ferrite powder ($NiFe_2O_4$) is highly reactive because of its strong CO adsorption [19]. NiO supported on ceria-alumina mixed oxides exhibited good catalytic performance at subzero temperatures [20]. Experimental studies and theoretical calculations have demonstrated that the introduction of Ni to Au catalysts can promote oxygen adsorption and activation on Au NPs [21,22]. Moreover, NiO prevents Au NPs from sintering during high temperature pretreatments [23].

Herein, for preparing an efficient novel catalyst based on Au/Al_2O_3 with improved catalytic performance and low Au loading, transition metal Ni was doped into the Al_2O_3 support as an additive for obtaining Au/Ni_xAl catalysts. The catalysts were tested for the CO oxidation reaction and characterized by XRD, TEM, H_2-TPR, O_2-TPD, and DRIFTS. The Ni content and pretreatment atmosphere of the catalysts were investigated to further understand the promotion effects of Ni species.

2. Experimental

2.1. Synthesis of the Ni_xAl supports

A series of Ni-doped Al_2O_3 supports were prepared using the precipitation-hydrothermal method, denoted as Ni_xAl, where x represented the molar ratio of Ni and Al. Considering the synthesis of $Ni_{0.05}Al$ as an example, 0.75 g $Al(NO_3)_3{\cdot}9H_2O$ and 0.03 g $Ni(NO_3)_2{\cdot}6H_2O$ were dissolved in 50 mL of deionized water, to which 50 mL of $(NH_4)_2CO_3$ solution (0.18 mol/L) was added. The obtained mixture with a pH of 9–10 was transferred into a 150 mL Teflon-lined stainless-steel autoclave and maintained at 100 °C for 24 h. After cooling to room temperature in air, the precipitants were centrifuged and washed with deionized water and ethanol, and subsequently dried at 80 °C. These precipitants were further calcined in air at 500 °C for 2 h at a heating rate of 1 °C/min to obtain the $Ni_{0.05}Al$ support. The pure Al_2O_3 support was prepared following the same steps without adding Ni precursors and is referred to as Al.

2.2. Preparation of the Au/Ni_xAl catalysts

The Au/Ni_xAl catalysts were prepared using the typical deposition-precipitation (DP) method with 1 wt% Au loading. The $HAuCl_4$ solution was added dropwise to an aqueous suspension of Ni_xAl, and the pH of the resulting mixture was adjusted to 8–9 using a $(NH_4)_2CO_3$ solution and maintained at 60 °C for 2 h. After washing and drying, the precursors were calcined under an air or H_2/N_2 atmosphere at 250 °C at a heating rate of 5 °C /min, to obtain the Au/Ni_xAl and Au/Ni_xAl-R catalysts, respectively.

2.3. Catalytic activity

The catalytic activity was evaluated using a fixed-bed quartz reactor using 50 mg of the catalyst. The total flow rate of the reaction gas was 67 mL/min with a composition of 1% CO, 20% O_2, and 79% N_2. The composition of the effluent gas was analyzed using an online GC-7890 gas chromatograph equipped with a thermal conductivity detector (TCD) and a 5 Å molecular sieve column. $T_{100\%}$ represents the temperature required for 100% CO conversion.

2.4. Catalyst characterization

XRD analysis of the samples was performed using an X'Pert3 powder diffractometer (Cu K_α, λ = 1.54056 Å). The diffraction patterns were collected using Cu K_α radiation (40 kV, 40 mA) over a 2θ range of 10°–90°. The Brunauer-Emmett-Teller (BET) surface area was measured using a Micromeritics Tristar 3000 instrument. The samples were degassed at 200 °C for 6 h before analysis and the nitrogen adsorption and desorption tests were subsequently performed at a liquid nitrogen temperature of –196 °C. Transmission electron microscopy (TEM) and high-angel annular dark field (HAADF) images of the catalysts were obtained using a Tecnai F30 electron microscope equipped with a FEG gun operating at 300 kV. The X-ray photoelectron spectroscopy (XPS) measurements were performed using a Thermo Scientific ESCALAB XI+ spectrometer.

H_2-TPR and O_2-TPD tests were performed using a Micromeritics Autochem II 2920 apparatus. For H_2-TPR, the precursors without further calcination were first treated at 100 °C under an Ar atmosphere for 60 min. After cooling to 50 °C, the samples were heated to 300 °C at a ramp rate of 10 °C/min under an 8% H_2/Ar flow. For O_2-TPD, the reduced catalysts were pretreated under an 8% H_2/Ar flow for 2 h at 250 °C before cooling to 40 °C. Next, the samples were exposed to a 5% O_2/He stream for 1 h. After blowing with He for 20 min, the temperature was then ramped to 500 °C at a heating rate of 10 °C/min.

FTIR experiments were conducted using a Bruker Vertex 70v spectrometer equipped with an MCT detector and ZnSe windows. The unpretreated samples were heated in the *in-situ* reaction cell to 250 °C for 30 min under air or H_2/Ar flow. After the background spectra were obtained at 30 °C under a He atmosphere, a flow of 5% CO/He was introduced into the cell for 20 min, which was then purged with He and the infrared spectra were recorded.

3. Results and discussion

The CO oxidation performance of the prepared Au/Ni_xAl catalysts is shown in Fig. 1a. After doping with Ni, the catalysts showed significantly higher CO conversion than that of Au/Al under the same reaction conditions, with the bare $Ni_{0.05}Al$ exhibiting negligible activity. The molar ratio of Ni/Al significantly influenced the reactivity, with increasing Ni/Al from 0.01 to 0.05, $T_{100\%}$ decreased from 100 to 40 °C. When Ni/Al was fur-

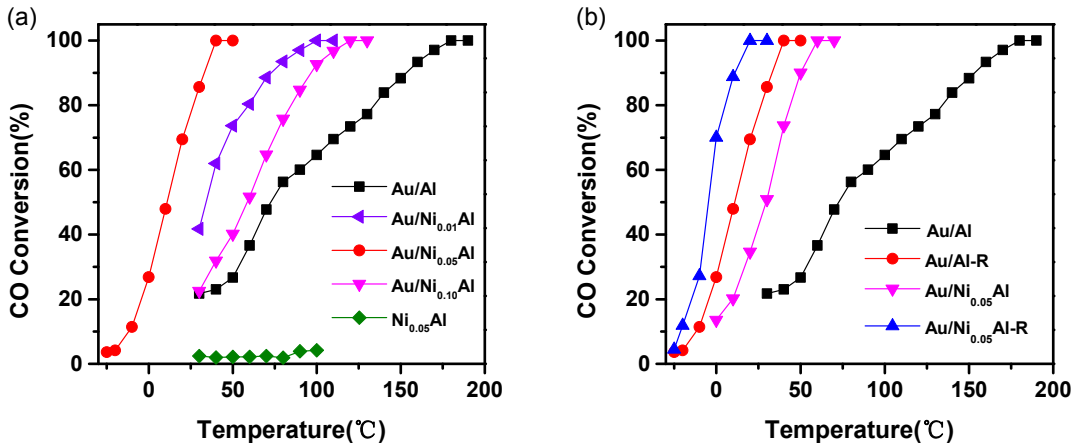

Fig. 1. CO conversion light-off curves over the prepared Au/Ni_xAl catalysts with different Ni/Al atomic ratios (a) and different pretreatment atmospheres (b).

ther increased to 0.1, $T_{100\%}$ increased to 120 °C. This indicates that the addition of a suitable amount of nickel can improve the activity of Au/Al for CO oxidation. Because the catalyst pretreatment atmosphere is also known to significantly influence catalytic activity [23,24], the reactivities of the catalysts pretreated under oxidative and reductive atmospheres were investigated (Fig. 1b). Au/$Ni_{0.05}$Al-R exhibited the best catalytic activity of the prepared samples with a $T_{100\%}$ of 20 °C, lower than that of Au/$Ni_{0.05}$Al ($T_{100\%}$ = 40 °C) and comparable with previously reported results (Table S1), whereas the $T_{100\%}$ of Au/Al-R was lower than that of Au/Al. These results indicated that the reductive catalyst pretreatment atmosphere improved the CO oxidation activity.

The textural properties of the different supports were measured by N_2 adsorption. As shown in Fig. 2a, the bare Al_2O_3 exhibited type IV nitrogen adsorption/desorption isotherms with H2-shaped hysteresis loops, suggesting the presence of typical ink-bottle mesopores. However, $Ni_{0.05}$Al showed type IV isotherms with H3-shaped hysteresis loops, indicating the presence of slit-shaped mesopores. The textural parameters of the different samples are summarized in Table S2. The specific surface areas were 404 and 297 m^2 g^{-1}, whereas the pore size distributions were centered at 4.5 and 10.1 nm for the Al_2O_3 and $Ni_{0.05}$Al, respectively. These results indicated that the co-precipitation influenced the final pore structure of the $Ni_{0.05}$Al and the crystalline structure. XRD patterns of the supports were measured to determine the influence of nickel on the crystal structure of Al_2O_3 and the results are shown in Fig. 2b. For bare Al_2O_3, two weak diffraction peaks at 45.8° and 67.3° were observed and were attributed to the γ-Al_2O_3 phase (COD 00-049-0134). After doping with Ni, the intensity of these diffraction peaks strengthened, and a broad peak at 37.2° appeared, which was attributed to the formation of Al_2O_3 with improved crystallinity [25]. Additional crystal nuclei formed during nucleation after doping with nickel. Thus, the crystal growth was facilitated in the hydrothermal reaction, resulting in larger crystalline grains and improved crystallinity [26]. After loading Au, the position of the diffraction peak remained unchanged and no peaks assigned to Ni species or Au NPs were detected, indicating that they were highly dispersed on the support.

TEM measurements were used to define the morphology of the as-synthesized catalysts and the gold particle sizes. Images of representative samples and the particle size distributions are

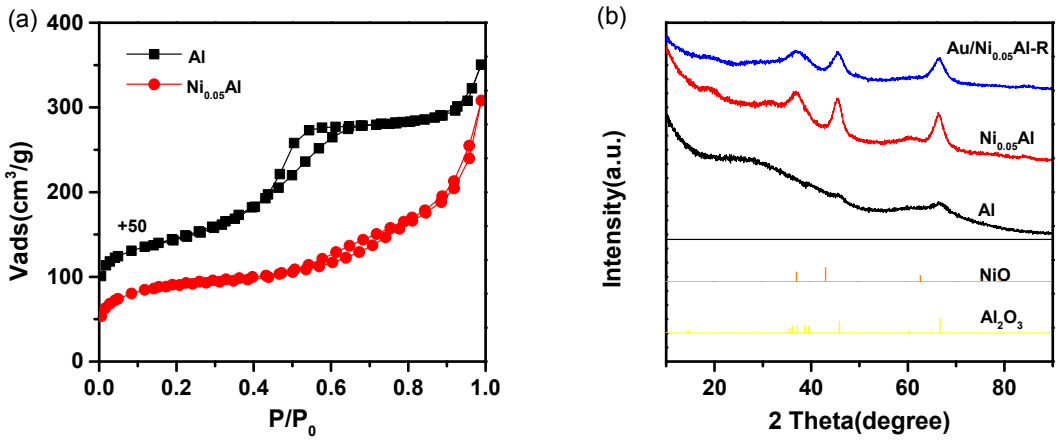

Fig. 2. (a) N_2 adsorption/desorption isotherms of the bare Al_2O_3 and $Ni_{0.05}$Al; (b) XRD patterns of the bare Al_2O_3, $Ni_{0.05}$Al and Au/$Ni_{0.05}$Al-R.

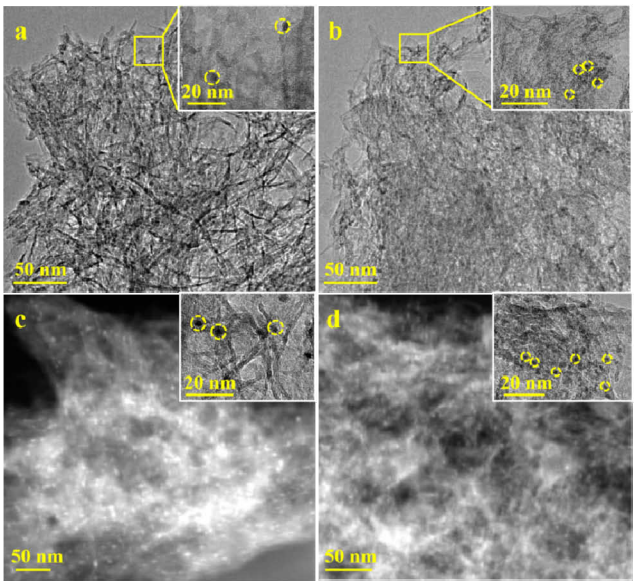

Fig. 3. TEM images of the Au/Al-R (a) and Au/$Ni_{0.05}$Al-R (b) samples; STEM-HAADF images of the 3 wt% Au/Al-R (c) and 3 wt% Au/$Ni_{0.05}$Al-R samples (d).

shown in Fig. 3a and 3b as well as Fig. S1. The Al_2O_3 support showed a closely packed sheet-like structure, which changed slightly after the introduction of Ni. For both catalysts, the Au NPs were highly dispersed on the support with average sizes of 3.6 and 2.4 nm for the Au/Al-R and Au/$Ni_{0.05}$Al-R samples, respectively. The high magnification images showed that the Au NPs supported on $Ni_{0.05}$Al were relatively small. To further distinguish the differences in particle size and distribution between the Au NPs supported on the different supports, the catalyst structure were studied with 3 wt% Au loading and the results are presented in Fig. 3c and 3d as well as Fig. S2. For the 3 wt% Au/$Ni_{0.05}$Al-R, the Au NPs were distributed much more uniformly than that of 3 wt% Au/Al and Au NPs larger than 5 nm were not observed. This indicated that the incorporation of Ni stabilized the small gold particles, resulting in a reduction of average size and uniform distribution of Au NPs, which may contribute to the improved activity. For Au/Al and Au/$Ni_{0.05}$Al, no obvious aggregated metallic NPs were observed in the TEM and HAADF images (Fig. S3), indicating high dispersions of both the Ni species and Au NPs.

H_2-TPR experiments were performed to elucidate the reduction properties of the precursors. As shown in Fig. 4a, the reduction peaks were centered at 205 and 189 °C for Au/Al and Au/$Ni_{0.05}$Al, respectively, which was attributed to the reduction of Au^{3+} to Au^0. The reduction peak of Au^{3+} shifted to lower temperatures when Ni was introduced, indicating that the Ni species improved the reducibility of Au in the precursors. It was previously reported that the incorporation of dopants with valence states below +4 results in higher lattice oxygen mobility which enhances the reduction processes [27]. Furthermore, O_2-TPD was performed to investigate the adsorbed oxygen species which are generally believed crucial for CO oxidation performance. According to Fig. 4b, the desorption peaks at 200–350 °C were mainly assigned to dissociatively adsorbed oxygen species (O^-) [28]. In this region, the desorption peak area of the Au/$Ni_{0.05}$Al-R catalyst was significantly larger than that of Au/Al-R, indicating that the incorporation of Ni remarkably enhanced the capacity for supplying oxygen species. Moreover, for Au/$Ni_{0.05}$Al-R, new desorption peaks appeared at 80 and 188 °C, arising from surface oxygen species weakly interacting with Au NPs and Ni species, respectively [24,29]. This phenomenon demonstrated that the Au/$Ni_{0.05}$Al-R adsorbed more active oxygen species and exhibited the strongest ability for utilizing oxygen species of all prepared catalysts, which coincided with catalytic performance and H_2-TPR results.

To understand the surface electron properties of the prepared Au catalysts, in situ FTIR analysis was performed using CO as probe molecule and the results are shown in Fig. 5a and 5b. After purging with He for 2 min, the band at approximately 2100 cm^{-1} was detected for both Au/Al-R and Au/$Ni_{0.05}$Al-R and was ascribed to the linear adsorption of CO on metallic Au [30]. For Au/$Ni_{0.05}$Al-R, a new band at approximately 2050 cm^{-1} was assigned to the adsorption of CO on Ni [31]. Upon purging with He, the bands at approximately 2100 cm^{-1} decreased gradually as a function of purging time. However, the peak intensity of Au/$Ni_{0.05}$Al-R decreased more slowly than that of Au/Al-R. The Au-CO band of Au/$Ni_{0.05}$Al-R remained after purging for 20 min, while the same band for Au/Al-R disap-

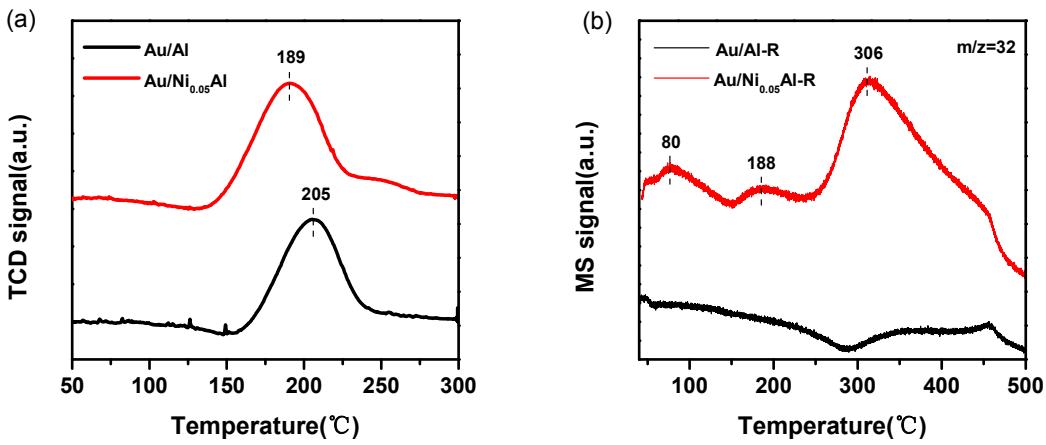

Fig. 4. H_2-TPR (a) and O_2-TPD (b) profiles of the prepared Au/Al_2O_3 and Au/Ni_xAl catalysts.

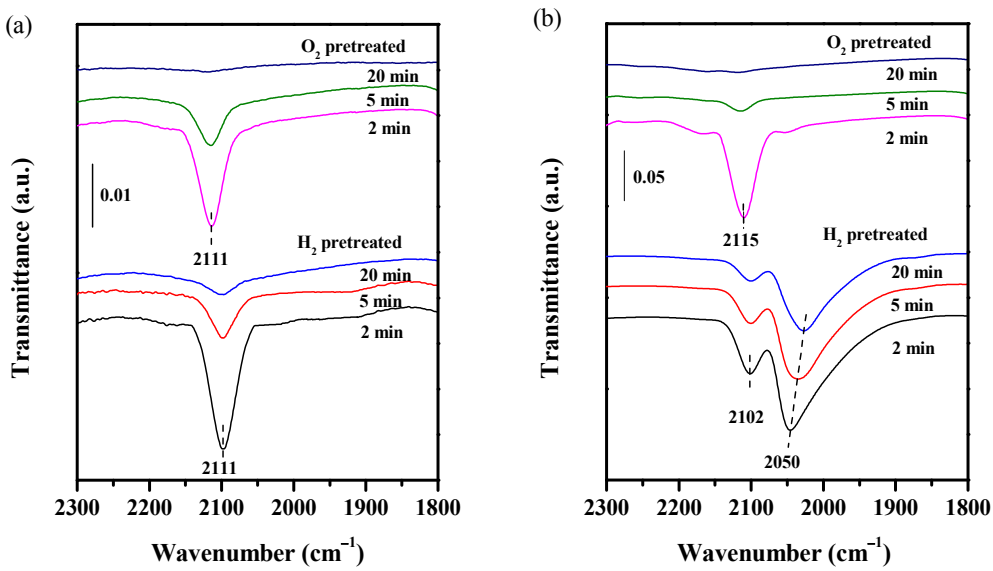

Fig. 5. In situ FTIR spectra of the Au/Al precursor (a) and Au/$Ni_{0.05}$Al precursor (b) pretreated at 250 °C after He purging for different durations.

peared under the same conditions. These results indicated that the electronic structure of the Au species was modified by Ni addition, resulting in stronger CO adsorption. The effect of the pretreatment atmosphere on the surface electron properties was also investigated [32]. Compared to the Au/$Ni_{0.05}$Al catalyst, the Au-CO band was red-shifted for Au/$Ni_{0.05}$Al-R, indicating the presence of more negatively charged Au species on the catalyst pretreated under a reductive atmosphere [30], leading to better CO oxidation reactivity.

To investigate the chemical state of the Au and Ni species, XPS experiments were performed and the results are shown in Fig. S4. The photoelectronic splitting of gold in Au/$Ni_{0.05}$Al-R showed binding energies located at 84.2 and 88.2 eV, which were assigned to the $4f_{7/2}$ and $4f_{5/2}$ orbitals of metallic gold, respectively. The main peaks of Au $4f_{7/2}$ and $4f_{5/2}$ in metallic gold are usually centered at 84.0 and 87.9 eV, respectively, and the slight shift to higher binding energy was attributed to electron transfer from Au to Ni [33]. For the Ni species, the Ni $2p_{3/2}$ spectra showed two peaks centered at 856.1 and 861.8 eV, a characteristic Ni $2p_{1/2}$ orbital band with a binding energy of 873.5 eV, and another sub-band at 879.9 eV. These bands were ascribed to the main peaks of NiO and corresponding satellite peak, respectively [23].

Because of the lack of oxygen mobility in Al_2O_3, the Langmuir-Hinshelwood mechanism is often assumed for CO oxidation over Au/Al_2O_3, for which CO adsorption and O_2 activation are both critical steps [34]. When the Au NPs were loaded onto the surface of Al_2O_3, CO oxidation occurred only on the Au NP surfaces. However, when Ni species were introduced into the framework of Al_2O_3, the synergetic effect between gold and nickel may result in higher catalytic activity. First, CO molecules could be adsorbed both on the surface of the Au NPs and nickel species, and the introduction of Ni distinctly strengthened CO adsorption on the Au NPs. Second, the presence of nickel formed new oxygen vacancies, allowing O_2 molecules to be adsorbed and activated more easily [33]. Third, the interaction between Au NPs and Ni_xAl decreased the size of the gold particles, which produced more active sites.

4. Conclusions

Herein, nickel-doped alumina nanosheets were synthesized via co-precipitation and used for the deposition of Au NPs. The obtained catalysts showed excellent performance for CO oxidation with 100% conversion of CO at 20 °C, much lower than that of the bare-Al_2O_3-supported Au catalyst. Combining TEM, H_2-TPR, O_2-TPD, and other characterization techniques, it was demonstrated that the incorporation of an optimized amount of Ni promoted the dispersion of Au NPs, strengthened CO adsorption, and provided reactive oxygen species to facilitate CO oxidation. Moreover, the catalysts pretreated under a reductive atmosphere facilitated CO oxidation. This study provides novel insights for developing other supports for heterogeneous catalysis.

References

[1] A. S. K. Hashmi, G. J. Hutchings, *Angew. Chem. Int. Ed.*, **2006**, 45, 7896–7936.
[2] M. Haruta, N. Yamada, T. Kobayashi, S. Iijima, *J. Catal.*, **1989**, 115, 301–309.
[3] T. Tabakova, L. Ilieva, I. Ivanov, R. Zanella, J. W. Sobczak, W. Lisowski, Z. Kaszkur, D. Andreeva, *Appl. Catal. B*, **2013**, 136–137, 70–80.
[4] J. Long, H. Liu, S. J. Wu, S. Liao, Y. Li, *ACS Catal.*, **2013**, 3, 647–654.
[5] M. Haruta, A. Ueda, S. Tsubota, R. M. T. Sanchez, *Catal. Today*, **1996**, 29, 443–447.
[6] G. Dong, J. C. Tseng, C. Weidenthaler, H. J Bongard, B. Spliethoff, W. Schmidt, F. Soulimani, B. M. Weckhuysen, F. Schüth, *J. Am. Chem. Soc.*, **2016**, 138, 9572–9580.
[7] A. Loubna, M. Boutahala, B. Djellouli, T. Dintzer, V. Pitchon, *Appl. Catal. A*, **2014**, 475, 446–460.

Graphical Abstract

Chin. J. Catal., 2020, 41: 350–356 doi: S1872-2067(19)63439-X

Promotion effects of nickel-doped Al_2O_3-nanosheet-supported Au catalysts for CO oxidation

Rao Lu, Lei He, Yang Wang, Xin-Qian Gao, Wen-Cui Li *
Dalian University of Technology

The Ni-doped Al_2O_3-supported Au catalyst exhibited excellent performance for CO oxidation because of its small Au NPs, strong CO adsorption, and O_2 activation properties.

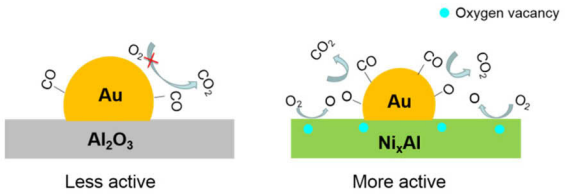

[8] D. Widmann, R. J. Behm, *Acc. Chem. Res.*, **2014**, 47, 740–749.
[9] M. Comotti, W. C. Li, B. Spliethoff, F. Schüth, *J. Am. Chem. Soc.*, **2006**, 128, 917–924.
[10] S. H. Overbury, V. Schwartz, D. R. Mullins, W. F. Yan, S. Dai, *J. Catal.*, **2006**, 241, 56–65.
[11] S. Carrettin, P. Concepcion, A. Corma, J. M. L. Nieto, V. F. Puntes, *Angew. Chem. Int. Ed.*, **2004**, 43, 2538–2540.
[12] H. L. Tang, Y. Su, B. S. Zhang, A. F. Lee, M. A. Isaacs, K. Wilson, L. Li, Y. G. Ren, J. H. Huang, M. Haruta, B. T. Qiao, X. Liu, C. Z. Jin, D. S. Su, J. H. Wang, T. Zhang, *Sci. Adv.*, **2017**, 3, e1700231.
[13] B. L. Moroz, P. A. Pyrjaev, V. I. Zaikovskii, V. I. Bukhtiyarov, *Catal. Today*, **2009**, 144, 292–305.
[14] C. X. Qi, H. J. Su, R. G. Guan, X. F. Xu, *J. Phys. Chem. C*, **2012**, 116, 17492–17500.
[15] J. Wang, K. Shang, Y. Guo, W. C. Li, *Microporous Mesoporous Mater.*, **2013**, 181, 141–145.
[16] C. X. Qi , S. D. Zhu, H. J. Su, H. Lin, R. G. Guan, *Appl. Catal. B*, **2013**, 138–139, 104–112.
[17] S. A. Nikolaev, E. V. Golubina, L. M. Kustov, A. L. Tarasov, O. P. Tkachenko, *Kinet. Catal.*, **2014**, 55, 311–318.
[18] H. J. Wu, G. Pantaleo, V. La Parola, A. M. Venezia, X. Collard, C. Aprile, L. F. Liotta, *Appl. Catal. B.*, **2014**, 156–157, 350–361.
[19] M. M. Rashad, O. A. Fouad, *Mater. Chem. Phys.*, **2005**, 94, 365–370.
[20] B. M. Reddy, K. N. Rao, P. Bharali, *Ind. Eng. Chem. Res.*, **2009**, 48, 8478–8486.
[21] B. D. Chandler, C. G. Long, J. D. Gilbertson, C. J. Pursell, G. Vijayarapharan, K. J. Stevenson, *J. Phys. Chem. C*, **2010**, 114, 11498–11508.
[22] C. C. Leon, J. G. Lee, S. T. Ceyer, *J. Phys. Chem. C*, **2014**, 118, 29043–29057.
[23] X. J. Xu, Q. Fu, X. G. Guo, X. H. Bao, *ACS Catal.*, **2013**, 3, 1810–1818.
[24] Y. X. Miao, L. Shi, L. N. Cai. W. C. Li, *Gold Bull.*, **2014**, 47, 275–282.
[25] F. R. Shamskar, F. Meshkani, M. Rezaei, *Ultrason. Sonochem.*, **2017**, 34, 436–447.
[26] F. R. Shamsker, M. Rezaei, F. Meshkani, *Int. J. Hydrogen Energy*, **2017**, 42, 4155–4164.
[27] R. Zanella, V. Rodríguez-Gonzalez, Y. Arzola, A. Moreno-Rodriguez, *ACS Catal.*, **2012**, 2, 1–11.
[28] B. F. Jin, Y. C. Wei, Z. Zhao, J. Liu, Y. Z. Li, R. J. Li, A. J. Duan, G. Y. Jiang, *Chin. J. Catal.*, **2017**, 38, 1629–1641.
[29] H. Q. Lu, L. Shi, C. He, W. Z. Weng, C. J. Huang, H. L. Wan, *Acta Phys.-Chim. Sin.*, **2012**, 28, 2697–2704.
[30] H. L. Tang, J. K. Wei, F. Liu, B. T. Qiao, X. L. Pan, L. Li, J. Y Liu, J. H. Wang, T. Zhang, *J. Am. Chem. Soc.*, **2016**, 138, 56–59.
[31] M. Q. Chai, X. Y. Liu, L. Li, G, X, Pei, Y. J. Ren, Y. Su, H. K. Cheng, A. Q. Wang, T. Zhang, *Chin. J. Catal.*, **2017**, 38, 1338–1346.
[32] C. T. Campbell, *Science*, **2004**, 306, 234–235.
[33] J. L. Guo, F. Dong, S. Y. Zhong, B. L. Zhu, W. P. Huang, S. M. Zhang, *Catal. Surv. Asia*, **2018**, 22, 208–221.
[34] J. Xu, Y. Q. Deng, Y. Luo, W. Mao, X. J. Yang, Y. F. Han, *J. Catal.*, **2013**, 300, 225–234.

镍掺杂对氧化铝纳米片负载金催化剂在CO氧化反应中的促进作用

路 饶, 贺 雷, 王 阳, 高新芊, 李文翠*
大连理工大学化工学院精细化工国家重点实验室, 辽宁大连116024

摘要: 负载型金催化剂在CO氧化反应中具有良好的低温活性, 受到了研究者的广泛关注, 其催化性能与载体的性质密切相关. 氧化铝具有廉价易得、比表面积大和热稳定性好等优点. 然而, 作为一种非还原性载体, 氧化铝提供活性氧物种的能力差, 与还原性载体相比催化剂的CO氧化活性较低. 理论计算和实验结果表明, 在金催化剂中引入过渡金属镍能够有效促进氧分子在催化剂表面的吸附和活化, 从而提升金催化剂活性. 此外, 过渡金属的存在能够提高金的分散度, 增加活性位数目, 防止在高温预处理过程中金颗粒的烧结, 从而提高催化剂的活性和稳定性.

基于上述考虑, 本文在氧化铝纳米片合成过程中原位引入硝酸镍, 以实现对氧化铝载体的改性, 然后负载金并应用于CO氧化反应. 结果表明, 当载体中的Ni/Al摩尔比为0.05, 金负载量为1 wt%时, 采用还原性气氛对催化剂进行预处理可以得到具有CO氧化性能优良的金催化剂, 20 °C下CO转化率即可达100%. 预处理气氛能够显著影响催化活性, 采用还原性气氛预处理后催化剂活性明显优于氧化性气氛预处理.

采用X射线衍射(XRD)、高分辨透射电镜(HRTEM)、氢气程序升温还原(H_2-TPR)、氧气程序升温脱附(O_2-TPD)、CO

吸附原位红外光谱(CO-DRIFT)和X射线光电子能谱(XPS)等表征手段进一步研究了镍掺杂对Au/Al_2O_3催化剂上CO氧化反应的促进作用机制. XRD测试未观察到明显的金或镍衍射峰, 表明金或镍物种均为高分散. HRTEM结果进一步证实, 引入镍物种后金颗粒的粒径由3.6 nm减小为2.4 nm, 表明镍掺杂有助于提高金的分散度. 而XPS结果显示, 镍掺杂催化剂中金与镍存在电子转移, 而镍仍以NiO为主. H_2-TPR结果表明, 镍掺杂的催化剂前驱体中的金物种更容易被还原. O_2-TPD结果证实, 镍掺杂催化剂能够引入更多的氧空位, 促进氧分子的吸附和活化, 从而促进CO氧化反应的进行. CO-DRIFT结果表明, 相比于氧化性气氛, 采用还原性气氛预处理后金物种的电子云密度增加, CO吸附增强. 而对于镍掺杂的催化剂, 金物种吸附CO分子的能力进一步提高, 有利于CO氧化反应的进行. 综上, 镍掺杂能够有效提高催化剂中金的分散度, 增强催化剂对CO的吸附, 促进氧气分子的吸附和活化, 从而提高了催化剂的CO氧化活性.

关键词: 氧化铝; 金催化剂; 镍掺杂; 一氧化碳氧化; 氧物种活化

收稿日期: 2019-05-10. 接受日期: 2019-06-23. 出版日期: 2020-03-05.

*通讯联系人. 电话: (0411)84986355; 电子信箱: wencuili@dlut.edu.cn

本文的电子版全文由Elsevier出版社在ScienceDirect上出版(http://www.sciencedirect.com/science/journal/18722067).